Direct interactions of mitotic arrest deficient 1 (MAD1) domains with each other and MAD2 conformers are required for mitotic checkpoint signaling

Received for publication, October 21, 2017, and in revised form, November 15, 2017 Published, Papers in Press, November 21, 2017, DOI 10.1074/jbc.RA117.000555

Wenbin Ji, Yibo Luo, Ejaz Ahmad, and Song-Tao Liu[1]

From the Department of Biological Sciences, University of Toledo, Toledo, Ohio 43606

Edited by Alex Toker

As a sensitive signaling system, the mitotic checkpoint ensures faithful chromosome segregation by delaying anaphase onset even when a single kinetochore is unattached to mitotic spindle microtubules. The key signal amplification reaction for the checkpoint is the conformational conversion of "open" mitotic arrest deficient 2 (O-MAD2) into "closed" MAD2 (C-MAD2). The reaction has been suggested to be catalyzed by an unusual catalyst, a MAD1:C-MAD2 tetramer, but how the catalysis is executed and regulated remains elusive. Here, we report that in addition to the well-characterized middle region of MAD1 containing the MAD2-interaction motif (MIM), both N- and C-terminal domains (NTD and CTD) of MAD1 also contribute to mitotic checkpoint signaling. Unlike the MIM, which stably associated only with C-MAD2, the NTD and CTD in MAD1 surprisingly bound both O- and C-MAD2, suggesting that these two domains interact with both substrates and products of the O-to-C conversion. $MAD1^{NTD}$ and $MAD1^{CTD}$ also interacted with each other and with the MPS1 protein kinase, which phosphorylated both NTD and CTD. This phosphorylation decreased the NTD:CTD interaction and also CTD's interaction with MPS1. Of note, mutating the phosphorylation sites in the $MAD1^{CTD}$, including Thr-716, compromised MAD2 binding and the checkpoint responses. We further noted that Ser-610 and Tyr-634 also contribute to the mitotic checkpoint signaling. Our results have uncovered that the $MAD1^{NTD}$ and $MAD1^{CTD}$ directly interact with each other and with MAD2 conformers and are regulated by MPS1 kinase, providing critical insights into mitotic checkpoint signaling.

The mitotic checkpoint is a crucial signal transduction pathway that contributes to faithful chromosome segregation (1–4). A single unattached kinetochore delays anaphase onset, underscoring the importance of signal amplification for the mitotic checkpoint (5). The conversion of mitotic arrest deficient 2 (MAD2)[2] domain from open (O-MAD2) to closed (C-MAD2) conformation is a well-recognized signal amplification mechanism for the mitotic checkpoint (6, 7). O-MAD2 is the predominant conformer in interphase cells (8, 9). During prometaphase, intracellular C-MAD2 concentration is increased to promote formation of the mitotic checkpoint complex (MCC), which binds and inhibits the anaphase promoting complex/cyclosome (APC/C) (1–4). In the current model, the MAD2 O–C conversion (*i.e.* O to C conversion) is catalyzed by a 2:2 MAD1:C-MAD2 tetramer localized at unattached kinetochores. Cytoplasmic O-MAD2 then heterodimerizes with the C-MAD2 moiety in the catalyst and morphs into C-MAD2. The reaction mechanism for the conversion is still unclear, but it may involve some intermediate folding states (I-MAD2) (6, 7, 10).

Two major questions remain unanswered for the model. First, human MAD1 is a mitotic checkpoint protein of 718 amino acid residues, but the formation of a 2:2 heterotetramer with C-MAD2 involves only its MAD2 interaction motif (MIM, 485–584 residues) especially a disordered loop spanning 530–550 residues (Fig. 1*a*) (11). However, some earlier and recent experiments argued for functional importance of the C-terminal domain of MAD1 (585–718 residues, $MAD1^{CTD}$) in maintaining the mitotic checkpoint (12–18). Moreover, even the MAD1 fragment encompassing 485–718 residues only exhibits low catalytic activity for MAD2 O–C conversion *in vitro* (12, 13, 19). The N-terminal domain of MAD1 (1–485 residues, $MAD1^{NTD}$) was thought to target the protein to nuclear envelope or kinetochores but may also interact with other proteins (20–23). Whether and how MAD1 domains outside MIM contribute to the checkpoint signaling warrants a revisit and careful investigation. Second, MAD1 forms a cell cycle independent complex with C-MAD2; how the complex only becomes an effective catalyst during prometaphase needs to be better defined (18, 24). Several kinetochore-localized mitotic kinases, including MPS1 kinase, were known to elevate C-MAD2 production, but direct biochemical evidence is still incomplete despite exciting recent progress (25–31).

Here we report our results targeting the above two questions. While our manuscript was prepared, two reports were published indicating that MPS1 phosphorylates MAD1 to enhance MAD2 O–C conversion and MCC assembly (29, 30). Our

This work was supported by National Institutes of Medicine Grant NIH R01CA169500 (to S.-T. L.). The authors declare that they have no conflicts of interest with the contents of this article. The content is solely the responsibility of the authors and does not necessarily represent the official views of the National Institutes of Health.

This article contains Figs. S1–S4 and Tables S1 and S2.

[1] To whom correspondence should be addressed. Tel.: 419-530-7853; E-mail: sliu@utnet.utoledo.edu.

[2] The abbreviations used are: MAD2, mitotic arrest deficient 2; O-MAD2, open MAD2; C-MAD2, closed MAD2; I-MAD2, intermediate MAD2; NTD, N-terminal domain; CTD, C-terminal domain; APC/C, anaphase promoting complex/cyclosome; MCC, mitotic checkpoint complex; MIM, MAD2-interaction motif; TEV, tobacco etch virus.

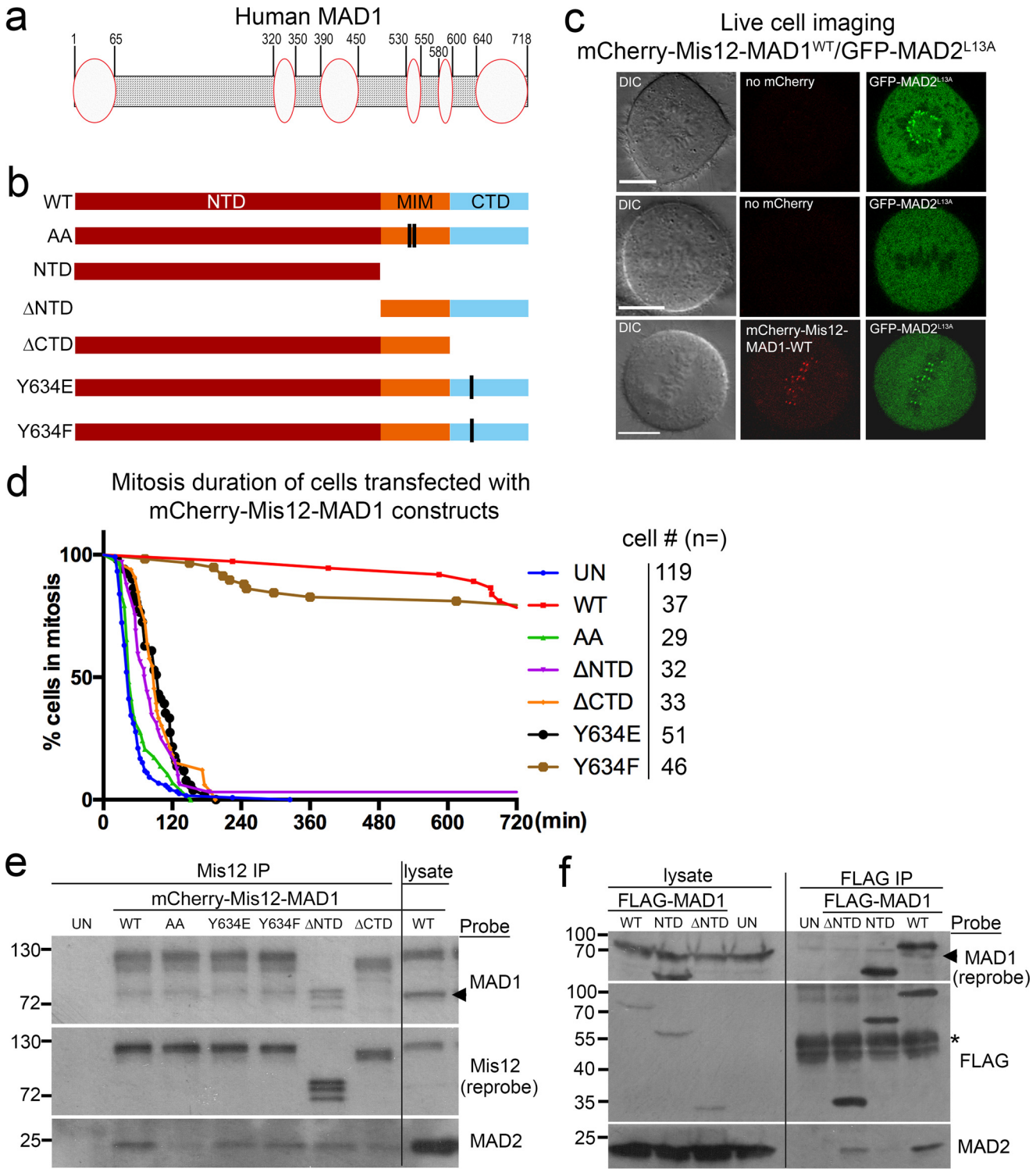

Figure 1. Both MAD1^{NTD} and MAD1^{CTD} are required for MAD1 activity. *a*, diagram of human MAD1 showing that multiple segments of MAD1 may form structures (*ovals*) other than coiled coils (*shaded area*). *b*, shown are various MAD1 mutants and truncations used for fusion with mCherry-Mis12. *c*, images of live cells either transfected with GFP-MAD2^{L13A} alone or together with mCherry-Mis12-WT MAD1. *DIC*, differential interference contrast. *Scale bar*, 10 μm. *d*, mitotic durations of HeLa cells either untransfected (*UN*) or transfected with mCherry-Mis12 fused with MAD1-WT, AA (defective in MAD2 binding because of mutations in MIM), ΔNTD, ΔCTD, Y634E, or Y634F were shown. Cell numbers imaged for each construct were listed on the right. *e*, lysates from control (*UN*) or transfected cells were subjected to anti-Mis12 immunoprecipitation (*IP*) followed by Western blots for Mis12-MAD1 fusions (probed with anti-Mis12 antibody), MAD2, and endogenous MAD1. Molecular weight markers are marked on the left (in kDa). The *arrow* indicates the position of endogenous MAD1. Although not always run as a full panel with all the mutants included, any parts of the results have been replicated at least three times by each of three investigators. *f*, lysates from control (*UN*) or FLAG-MAD1 transfected cells were subjected to anti-FLAG immunoprecipitation and then probed for MAD1 and MAD2. The *asterisk* indicates IgG heavy chain.

results support the importance of MAD1 Thr-716 phosphorylation, but we have also uncovered other protein-protein interactions between MAD1, MAD2, and MPS1 and the phosphorylation-dependent regulation of some of the interactions. Our work highlights the coordination of different MAD1 domains in efficient mitotic checkpoint signaling and provides further mechanistic insights into the MAD2 O–C conversion reaction.

Results

MAD1 N-terminal and C-terminal domains (NTD and CTD) are required for efficient mitotic checkpoint signaling

In studying the MAD2 O–C conversion, earlier work has detailed the conformational changes of MAD2 (6, 32). We reasoned that better characterization of the MAD1:C-MAD2 catalyst would provide further mechanistic insights into the conversion reaction and hence the signal amplification step of the mitotic checkpoint. We noted that even though MAD1 is commonly depicted as a rigid coiled-coil protein, parts of its NTD and CTD have been shown or predicted to remain disordered or adopt other structures (Fig. 1*a* and Fig. S1) (11, 33, 34). We first investigated the possible contribution of $MAD1^{NTD}$ and $MAD1^{CTD}$ to the mitotic checkpoint using a "separation of function" system developed by Maldonado and Kapoor (26). In this system, an mCherry-Mis12-MAD1 fusion construct was exploited to examine catalytic efficiency of the MAD1:C-MAD2 catalyst without concerns over the kinetochore targeting aspect of its regulation (26) (Fig. 1*b*). Although endogenous MAD1 and MAD2 disappeared from metaphase kinetochores which presumably were occupied by spindle microtubules, expression of wild-type MAD1 ($MAD1^{WT}$) fused with constitutive kinetochore protein Mis12 retained MAD1 at the metaphase plate and recruited GFP-$MAD2^{L13A}$ to these metaphase kinetochores (26, 28) (Fig. 1*c* and Fig. S2). $MAD2^{L13A}$ is a MAD2 mutant locked in C conformation (13, 32). The persistence of MAD1 and MAD2 at metaphase attached kinetochores was sufficient to trigger a >12-h mitotic arrest in HeLa cells (26, 28) (Fig. 1*d*). The arrest was dependent on C-MAD2 binding to MAD1, as cells expressing the fusion with MAD2-binding–deficient $MAD1^{AA}$ mutant (K541A, L543A in MIM) finished mitosis within ~60 min on average (Fig. 1*d* and Fig. S2) (26). Note no GFP-$MAD2^{L13A}$ was localized at metaphase kinetochores containing mCherry-Mis12-$MAD1^{AA}$, although GFP-$MAD2^{L13A}$ did appear at the last few unattached kinetochores, most likely because of presence of endogenous MAD1 there (Fig. S2, compare the second and third columns). Furthermore, co-expression of $MAD2^{\Delta C10}$, an O-conformer locked mutant of MAD2 (6, 7), abolished the mitotic arrest in $MAD1^{WT}$ transfected cells (data not shown), corroborating that the arrest was because of O–C conversion–dependent checkpoint responses (28, 35, 36).

Consistent with previous reports (14–17), MAD1 missing 597–718 residues ($MAD1^{\Delta CTD}$), even as a fusion with Mis12, could not maintain mitotic arrest (98 ± 7 *versus* 749 ± 22 min for $MAD1^{WT}$, mean ± S.D., $p < 0.0001$, Student's *t* test, there might be an underestimation for $MAD1^{WT}$ transfected cells as the movies lasted only 13 h). Moreover, a specific $MAD1^{Y634E}$ mutant also abolished the mitotic arrest, whereas a $MAD1^{Y634F}$ mutant did not significantly impact mitotic duration (Fig. 1*d*). Tyr-634 is situated close to the junction between the coiled-coil subdomain (597–637 residues) and the globular subdomain (638–718 residues) of the $MAD1^{CTD}$ (33). We noticed this site during screening potential MAD1 phosphomutants as Tyr-634 was reported to be phosphorylated *in vivo* (37). Interestingly, MAD1 missing 1–485 residues ($MAD1^{\Delta NTD}$) could not maintain prolonged mitosis either (average duration, 101 ± 22 min) (Fig. 1*d*).

We then examined the association of different mCherry-Mis12-MAD1 fusion proteins with endogenous MAD1 and MAD2 by Mis12 immunoprecipitation. Little MAD2 was found to associate with $MAD1^{AA}$ as predicted; steady-state levels of MAD2 binding to other MAD1 mutants were also slightly reduced (Fig. 1*e*). The reduction of MAD2 binding became more obvious for some mutants when FLAG immunoprecipitation was performed using cells transfected with FLAG-tagged MAD1 constructs (Fig. 1*f*). In addition, $MAD1^{\Delta CTD}$ and $MAD1^{\Delta NTD}$ did not interact with endogenous MAD1, indicating a dimerization defect (Fig. 1, *e* and *f*; note that mCherry-Mis12-$MAD1^{\Delta NTD}$ runs at the same position as endogenous MAD1. More on MAD1 dimerization in the last section of "Results"). Taken together, the results shown in Fig. 1 have confirmed the important role of $MAD1^{MIM}$, but also revealed that both NTD and CTD of MAD1 are required for an efficient mitotic checkpoint.

$MAD1^{NTD}$ and $MAD1^{CTD}$ bind to both O-MAD2 and C-MAD2

We hypothesized that the NTD and CTD of MAD1 facilitate mitotic checkpoint responses by enhancing MAD2 O–C conversion. Based on the analogy to an isomerase which at least transiently interacts with its substrate and product, we prepared recombinant proteins and examined potential interactions between GST-tagged $MAD1^{NTD}$ or $MAD1^{CTD}$ with untagged O- or C-MAD2, supplied as $MAD2^{\Delta C10}$ or $MAD2^{L13A}$ conformation-locked mutants, respectively (6, 7, 36) (Fig. 2*a*). When proteins were used at roughly endogenous concentrations (see "Experimental Procedures"), GST-pulldown results showed that NTD and CTD bound to both conformers of MAD2 (Fig. 2*b*, *lanes 1*, *3* and *5*, *7*). Under similar conditions, the $MAD1^{MIM}$ only bound to C-MAD2, just as reported previously (compare MAD2 in Fig. 2*b*, *lanes 2* and *6*) (11, 38). The conformational status of the O- and C-MAD2 mutants was further verified, because only $MAD2^{L13A}$ bound to GST-$CDC20^{(111–138)}$ or GST-$BUBR1^{(1–371)}$, also as reported before (36, 38) (Fig. S3). The novel interactions were not mediated by tags, as GST alone did not pull down any MAD2 (Fig. 2*b*, *lanes 4* and *8*). Importantly, GFP-$MAD2^{\Delta C10}$ was found to be recruited to centromeres in interphase cells expressing mCherry-Mis12-MAD1 fusions, supporting the idea that the interaction between O-MAD2 and MAD1, although surprising, could happen in cells (Fig. 2*c*, $MAD1^{\Delta CTD}$ used here). Maintaining MAD1 fragments at the endogenous concentration of 60 nM, titrating GST pulldown experiments found that binding of MAD2 to NTD, MIM, and CTD could be detected when MAD2 concentrations were as low as 30 nM. Estimations of the half-maximal binding concentrations of $MAD1^{CTD}$ with

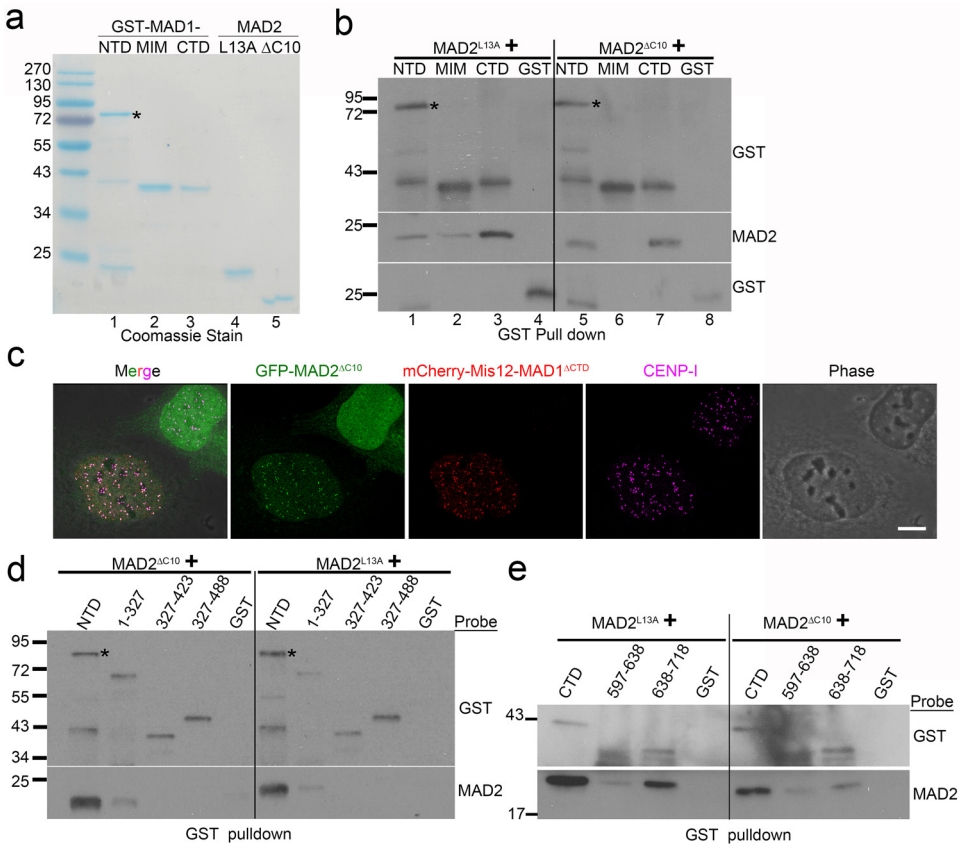

Figure 2. MAD1^{NTD} and MAD1^{CTD} interact with both O-MAD2 and C-MAD2. *a*, Coomassie Blue stain after SDS-PAGE of purified recombinant proteins. GST-NTD tends to be more labile for degradation. The *asterisk* marks expected size of GST-NTD. *b*, GST-tagged MAD1^{NTD}, MIM, CTD, or GST alone were incubated with either MAD2^{L13A} or MAD2$^{\Delta C10}$, and GST pulldown assays were followed by Western blotting of GST and MAD2. The final concentrations of GST or GST-tagged MAD1 fragments were 60 nM, whereas those of MAD2 mutants were 230 nM. Similar results have been replicated for at least five times by two investigators, using different batches of protein preparations. *c*, immunofluorescence of two interphase cells transfected with GFP-MAD2$^{\Delta C10}$. Note that the GFP signals are recruited to centromeres only in the cell co-expressing mCherry-Mis12-MAD1$^{\Delta CTD}$. Centromeres are stained with anti-CENP-I antibody. *Scale bar*, 10 μm. *d*, GST-tagged MAD1 N-terminal truncations were incubated with MAD2$^{\Delta C10}$ or MAD2^{L13A} followed by GST pulldown assays. The result is representative of four replicates. *e*, GST-tagged MAD1^{CTD} coiled-coil subdomain (597–638 residues) or globular subdomain (638–718 residues) were incubated with MAD2$^{\Delta C10}$ or MAD2^{L13A} followed by GST pulldown and Western blotting. The result is representative of three replicates by two investigators based on different batches of proteins.

C-MAD2 and O-MAD2 fell in the range of 100–250 nM (Fig. S3).

We attempted to further define the regions on MAD1^{NTD} or MAD1^{CTD} responsible for association with MAD2. Several MAD1^{NTD} or MAD1^{CTD} truncations produced either insoluble or heavily degraded proteins (data not shown). However, testing with MAD1^{NTD} truncations that we were able to purify, including MAD1$^{(1-327)}$, MAD1$^{(327-423)}$, and MAD1$^{(327-488)}$, revealed dramatically reduced MAD2-binding capability of these fragments (Fig. 2*d*). The globular subdomain (638–718 residues) of MAD1^{CTD} retained approximately half the MAD2-binding capacity of MAD1^{CTD} whereas the coiled-coil subdomain in the CTD showed only residual binding (Fig. 2*e*). These combined results suggest that the integrity of MAD1^{NTD} or MAD1^{CTD} is crucial for binding to O-MAD2 or C-MAD2.

A novel interface in MAD2 is employed for its association with NTD or CTD of MAD1

A MAD2 molecule has two well-characterized interfaces for protein-protein interactions: the "safety belt" characteristic of C-MAD2 conformation to which MAD1^{MIM} and CDC20 bind (11, 38–40), and the dimerization domain (primarily αC helix) that allows MAD2 to form O:C or C:C dimers or interact with p31^{comet} or BUBR1 (13, 32, 36, 41, 42). NTD and CTD of MAD1 bound to both MAD2$^{\Delta C10}$ and MAD2^{L13A}, suggesting no discrimination against either MAD2 conformation (Fig. 2*b*). To further support this notion, wild-type MAD2, which exists as a mixture of both O and C conformers (8), bound to all three MAD1 fragments, whereas another MAD2 mutant MAD2^{S195D}, predominantly in O conformation (43), bound to MAD1^{NTD} or MAD1^{CTD} but not MAD1^{MIM} (Fig. 3*a*, compare the *left* and *middle panels*). On the other hand, MAD2^{LARQ} (L13A/R133E/Q134A), a dimerization defective C-MAD2 mutant (36), associated with MAD1^{NTD} or MAD1^{CTD} at similar levels as MAD2^{L13A} (Fig. 3*b*). MAD2$^{\Delta N10}$, which might mimic an intermediate conformation during O to C MAD2 conversion (10), bound to all three MAD1 fragments (Fig. 3*c*). The above results suggest that the safety belt (or C conformation), the dimerization domain (at least the RQ mutant), or the N-terminal 10 amino acids are not essential for MAD2 to interact with MAD1^{NTD} or MAD1^{CTD}. Therefore, a novel interface on MAD2, possibly shared by both O and C conformers, is employed for interactions with MAD1^{NTD} and MAD1^{CTD}.

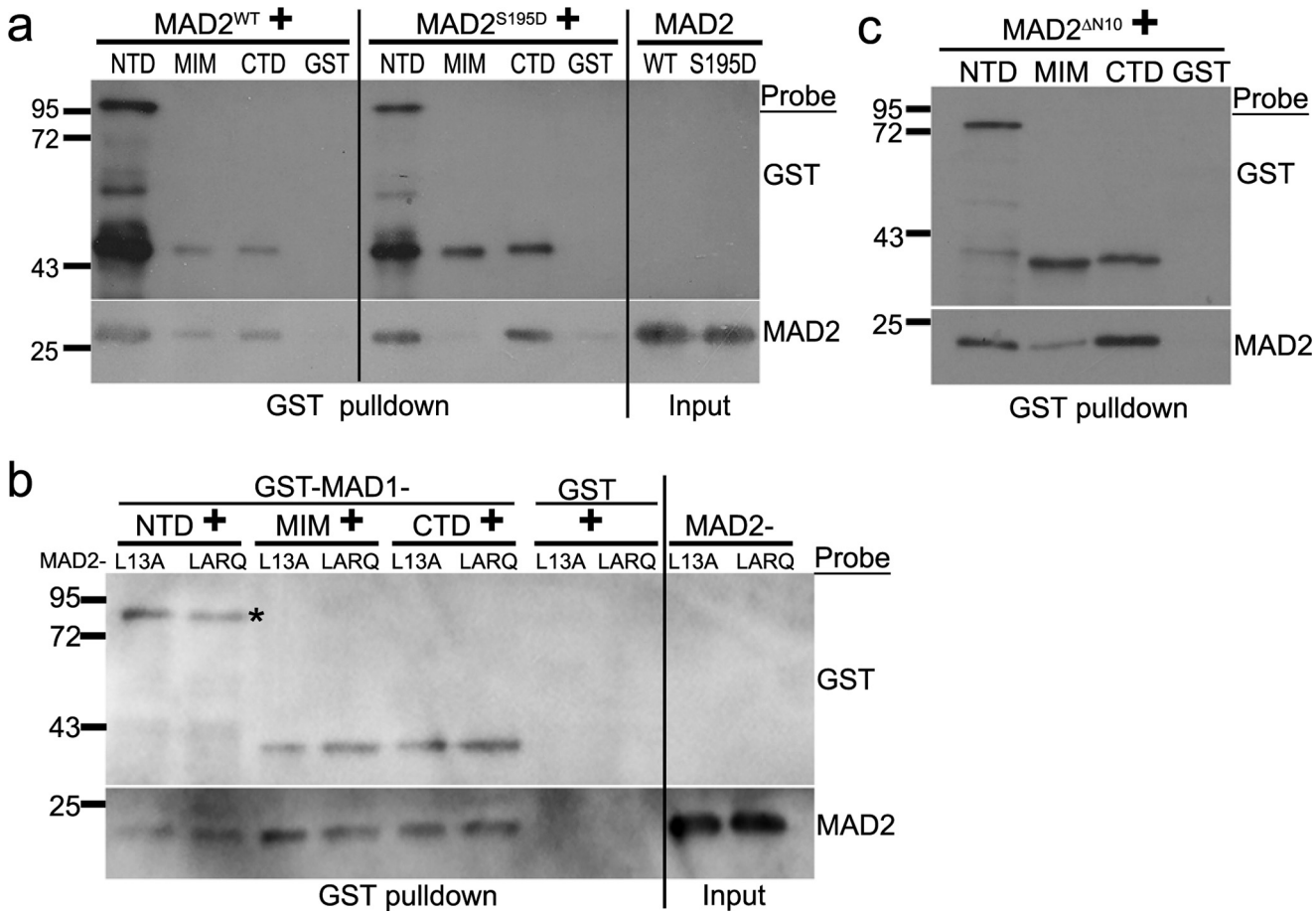

Figure 3. A novel interface in MAD2 is employed for its association with NTD or CTD of MAD1. *a*, GST-pulldown assays using GST-tagged MAD1 fragments after incubation with His_6-tagged wild type MAD2 ($MAD2^{WT}$) or $MAD2^{S195D}$ mutant. *b*, GST-pulldown assays using GST-tagged MAD1 fragments with $MAD2^{L13A}$ and $MAD2^{LARQ}$. The *asterisk* marks expected size of GST-NTD. The result is representative of four replicates. *c*, GST-pulldown assays using GST-tagged MAD1 fragments with $MAD2^{\Delta N10}$.

MPS1 kinase phosphorylates $MAD1^{NTD}$ and $MAD1^{CTD}$

It is known that the kinase activity of MPS1 is essential for maintaining mitotic arrest even when MAD1 constitutively localizes at kinetochores as a fusion with mCherry-Mis12 (25–28). We hypothesized that MPS1 might phosphorylate MAD1 or MAD2 to regulate the efficiency of the MAD1:C-MAD2 catalyst. *In vitro* kinase assays found that MPS1 indeed phosphorylated $MAD1^{NTD}$ and $MAD1^{CTD}$ (Fig. 4*a*, compare *lanes 3* and *5* in both the *Coomassie Blue stain panel* and the *autoradiography panel*). The specificity of the kinase assay was validated by the fact that reversine, a previously characterized MPS1 inhibitor (44), reduced *in vitro* phosphorylation of an artificial MPS1 substrate myelin basic protein (Fig. 4*a*, compare *lanes 1* and 2 in the *right panel*). GST alone, GST-$MAD1^{MIM}$, and MAD2 conformers ($MAD2^{L13A}$ and $MAD2^{\Delta C10}$) were not good substrates for MPS1 under the experimental condition (Fig. 4*a*, *lanes 4* and *6-8*). Interestingly, recombinant MPS1 kinase binds to $MAD1^{NTD}$ or $MAD1^{CTD}$ but not MIM in the absence of ATP (Fig. 4*b*, note the presence of MPS1 signal in *lanes 1* and *3* but not in *lanes 2* and *4*).

We then tested whether MPS1 phosphorylation affects the interactions between $MAD1^{CTD}$ and MAD2 conformers. We focused on CTD because it was not only easily purified without apparent degradation but also showed functional significance (see below). We did notice that GST-MPS1 but not GST alone could also bind to $MAD2^{L13A}$ and $MAD2^{\Delta C10}$ (Fig. 4*c*). *In vitro* incubation of MPS1, CTD, and MAD2 led to phosphorylation of CTD, as evidenced by the mobility shift detected by anti-His_6 antibody, and positive signals of phospho-Thr antibody (Fig. 4, *d* and *e*, *lane 1*). However, the association of either $MAD2^{L13A}$ or $MAD2^{\Delta C10}$ with CTD did not show obvious changes when compared with reactions in the absence of ATP or in the presence of MPS1 inhibitor reversine (Fig. 4, *d* and *e*, compare MAD2 signals in *lanes 1–3*). The interactions between phosphorylated CTD and MPS1, nevertheless, became weaker (Fig. 4, *d* and *e*, compare MPS1 signals in *lanes 1–3*). ATP, reversine, and DMSO (solvent control) did not affect the interactions between CTD and MAD2 conformers (Fig. 4, *d* and *e*, *lanes 4–6*).

Functional characterization of MPS1 phosphorylation sites on MAD1

Realizing some limitations of *in vitro* binding experiments especially with protein fragments, we decided to directly test the potential effects of MPS1 phosphorylation on MAD1 in cells. Through mass spectrometry we identified eight *in vitro* MPS1 phosphorylation sites on $MAD1^{NTD}$ and $MAD1^{CTD}$. The sites are Thr-8, Ser-22, Ser-62, Thr-323, Ser-598, Ser-610,

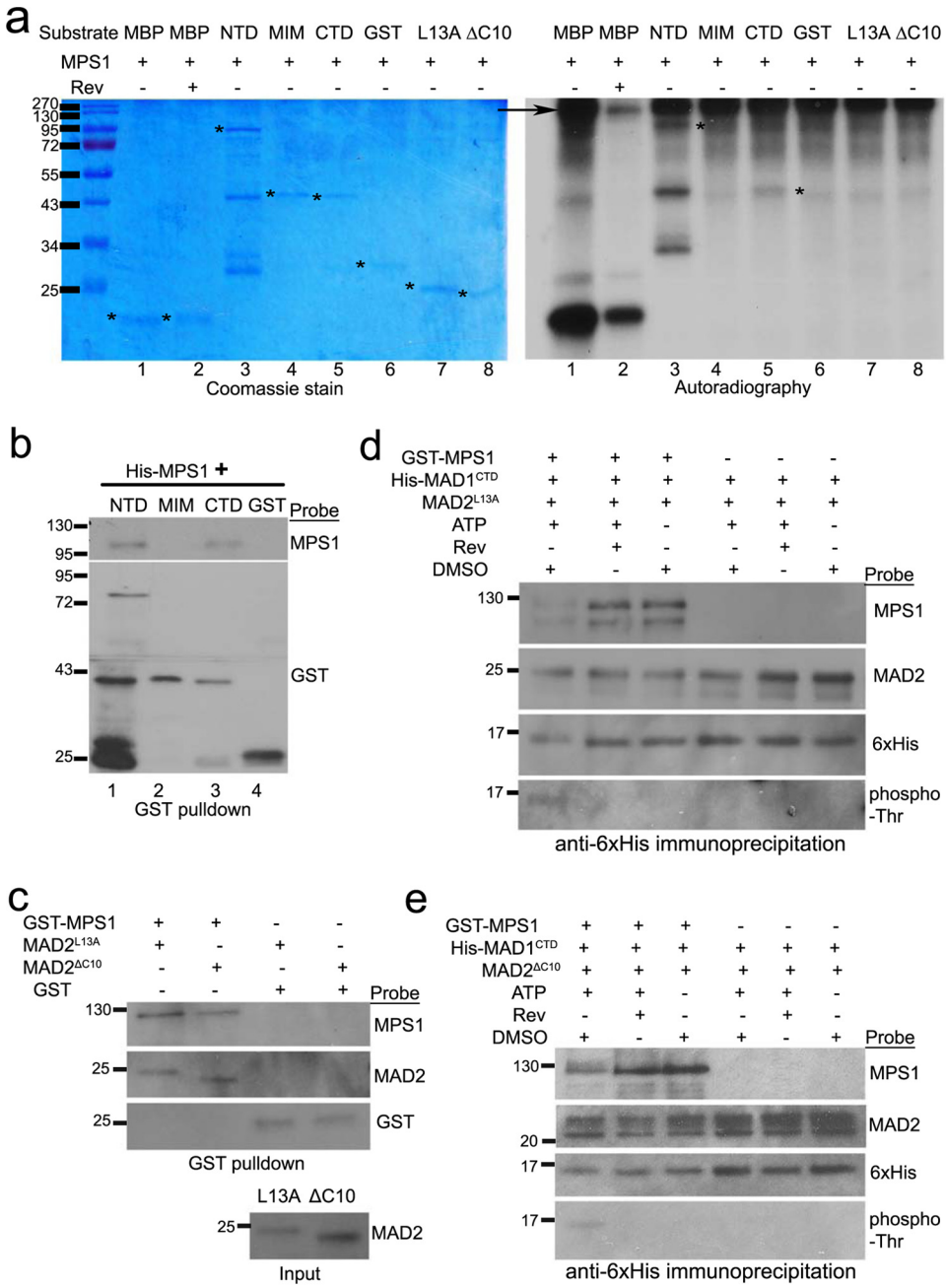

Figure 4. MPS1 phosphorylates MAD1 and interacts with MAD1 and MAD2. *a*, *in vitro* kinase assays were performed using recombinant GST-MPS1, with myelin basic protein as an artificial substrate of MPS1, or with GST-MAD1^{NTD}, MAD1^{MIM}, MAD1^{CTD}, untagged MAD2^{L13A}, or MAD2$^{\Delta C10}$. The SDS-PAGE gel of the kinase assays were stained with Coomassie Blue (*left*). Phosphorylation of the proteins by MPS1 was detected by autoradiography after the gel was dried (*right*). The *asterisks* indicate the expected sizes of corresponding proteins. The *arrow* indicates GST-MPS1. Reversine (*Rev*) was used in *lane 2* to validate the kinase specificity. *b*, GST-pulldown assays using GST or GST-tagged MAD1 fragments (~80 nM final concentration) after incubation with His-tagged MPS1 (~40 nM). The binding reactions did not contain ATP. The result is representative of at least three replicates by two investigators. *c*, GST-pulldown assays using GST or GST-tagged MPS1 (~60 nM) after incubation with untagged MAD2$^{\Delta C10}$ or MAD2^{L13A} (both at 230 nM final concentrations). The binding reactions did not contain ATP. The result is representative of at least three replicates by two investigators. *d* and *e*, immunoprecipitation using anti-His$_6$ antibody (1 μg) to detect His-tagged MAD1^{CTD} interactions with untagged MAD2^{L13A} (*d*) or MAD2$^{\Delta C10)}$ (*e*) after incubation in the presence/absence of GST-MPS1 kinase, ATP, or MPS1 inhibitor reversine. All recombinant proteins in the incubation reactions were used at final concentrations equivalent to their endogenous levels. The results have been replicated five times.

Thr-624, and Thr-716 (Fig. 5*a*). To test the importance of these sites in cells, a mCherry-Mis12-MAD1^{8A} mutant with all the sites mutated into alanine was expressed and found to be defective in maintaining the mitotic arrest (229 ± 23 min mitotic duration) (Fig. 5*b*). Mutating all four NTD sites into alanine showed no effect, but alanine mutants at the four CTD sites (MAD1^{CTD4A}) shortened the mitotic duration comparable with MAD1^{8A} (Fig. 5*b*). Further tests found that little CTD^{4A} is phosphorylated when compared with wild-type CTD (CTD^{WT}) *in vitro*, supporting that the CTD four sites, Ser-598, Ser-610, Thr-624 and Thr-716, constituted primary phosphorylation sites of MPS1 kinase under our *in vitro* experimental conditions (Fig. S4*a*).

Next, a mCherry-Mis12-MAD1^{CTD4E} phosphomimic mutant was prepared and surprisingly found to be also defective in

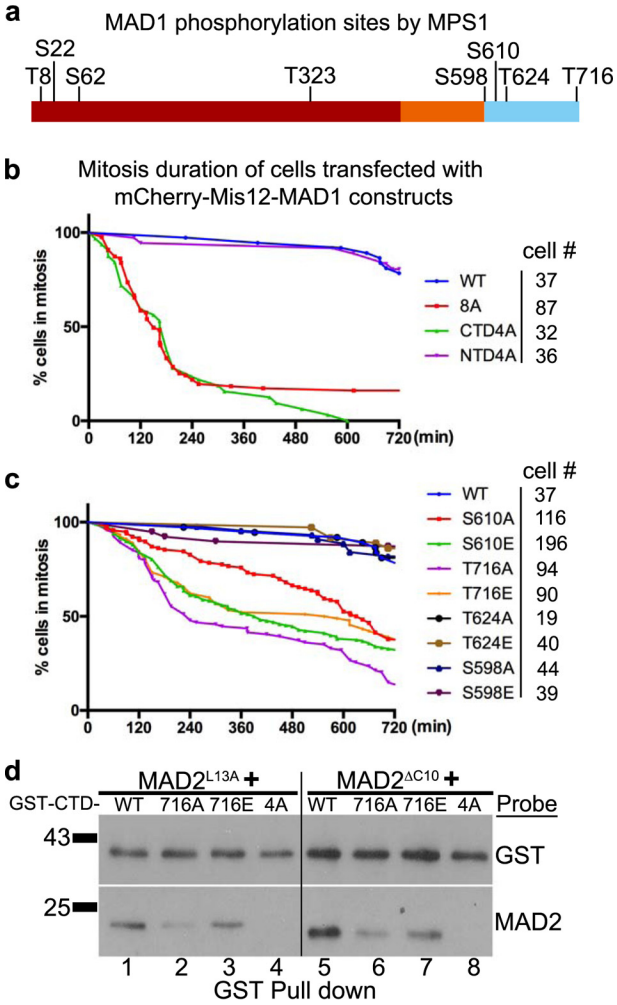

Figure 5. The putative MPS1 phosphorylation sites on MAD1^{CTD} are required for the mitotic checkpoint. *a*, MAD1 phosphorylation sites by MPS1 kinase *in vitro* as determined by mass spectrometry. *b*, mitotic durations of HeLa cells transfected with mCherry-Mis12 fused with MAD1^{WT}, MAD1^{8A} (Thr-8, Ser-22, Ser-62, Thr-323, Ser-598, Ser-610, Thr-624, Thr-716 to A), MAD1^{NTD4A} (full length but Thr-8, Ser-22, Ser-62, Thr-323 to A) or MAD1^{CTD4A} (full length but Ser-598, Ser-610, Thr-624, Thr-716 to A). Cell numbers imaged for each construct are listed on the right. *c*, phosphomimic and phosphoresistant mutants at individual MPS1 phosphorylation sites in the MAD1^{CTD} (Ser-598, Ser-610, Thr-624, Thr-716) were prepared as mCherry-Mis12 fusion constructs and transfected HeLa cells were imaged for mitotic durations as in (*b*). *d*, GST-tagged MAD1^{CTD} fragments in WT, or containing T716A or T716E or CTD-4A mutations (~240 nM) were incubated with either MAD2^{L13A} or MAD2$^{\Delta C10}$ (230 nM), then GST pulldowns were probed with anti-GST and anti-MAD2 antibodies.

maintaining the mitotic arrest (Fig. S4*b*). We reasoned that, for a functional mitotic checkpoint in cells, one or more of the four residues identified through *in vitro* kinase assays could not tolerate mutations. Both phosphoresistant and phosphomimic mutants at individual sites were then prepared. The mutants at Ser-598 or Ser-624 did not show obvious defects in mitotic checkpoint responses when fused with mCherry-Mis12. However, the mutants at Ser-610 and Thr-716 showed significant differences in mitotic arrest durations when compared with the MAD1^{WT} fusion (Fig. 5*c*). Furthermore, the T716E mutant maintained the checkpoint longer than the T716A mutant (441 ± 38 *versus* 242 ± 48 min, $p < 0.05$, Student's *t* test), indicating that Thr-716 is likely the residue activated by MPS1 for mitotic checkpoint signaling. However, the mCherry-Mis12 fusion of MAD1^{T716E} mutant could not maintain mitotic arrest when transfected cells were challenged by reversine (Fig. S4*c*), suggesting either the phosphomimic mutant is imperfect or MPS1 has additional key substrates required for a functional mitotic checkpoint.

To further understand the imaging results with different CTD mutants, we examined whether these mutants affected the interaction of MAD1^{CTD} with MAD2. Both CTD^{4A} and CTD^{4E} showed defects in binding to O-MAD2 and C-MAD2 (Fig. S4*d*). Furthermore, CTD^{T716A} bound less O-MAD2 and C-MAD2 as compared with CTD^{WT} or CTD^{T716E} (Fig. 5*d*). Similarly, the functional defective MAD1^{Y634E} mutant also bound to less O-MAD2 and C-MAD2 than MAD1^{Y634F} (Fig. S4*e*). These results correlate mitotic arrest durations with the capability of MAD1^{CTD} mutants to bind to MAD2 (Figs. 1*d* and 5 and Fig. S4).

MPS1 phosphorylation of MAD1 modulates interdomain and intermolecular interactions

Because MIM, CTD, and NTD of MAD1 are all required for an effective mitotic checkpoint (Fig. 1), we next investigated whether there is coordination among these domains. The presumed non–coiled-coil domains along the length of MAD1 might provide certain bends and turns to the molecule, and an earlier model has suggested that MAD1^{CTD} folds back to the proximity of the catalytic core consisting of MIM and associated C-MAD2 (11). We found that NTD directly interacted with CTD (Fig. 6, *a*, *lane 1* and *b*, *lane 2*). CTD interacted with itself (Fig. 6*a*, *lane 3*), agreeing with published crystal structure (PDB: 4DZO) and acting as a positive control in this binding assay (33). MIM does not directly interact with CTD or NTD (Fig. 6, *a*, *lane 2* and *b*, *lane 1*). Addition of MPS1 kinase reduced the interactions between MAD1^{NTD} and MAD1^{CTD} (Fig. 6*c*). The effect depended on the MPS1 kinase activity as omitting ATP from the reactions or adding MPS1 inhibitors (reversine or AZ3146) reversed the MPS1 effect on NTD:CTD interaction (Fig. 6*c*, compare His signals in *lane 2* and those in *lanes 3–5*).

MAD1 dimerization has been observed in MAD1^{MIM}:MAD2 and MAD1^{CTD} crystal structures (PDB: 1GO4 and 4DZO, respectively) (11, 33). However, whether MAD1 dimerization is essential for its activity to promote MAD2 O–C conversion is unclear. We noticed that in Fig. 1, *e* and *f*, MAD1 truncations missing either NTD or CTD did not co-immunoprecipitate endogenous MAD1 as well as other fusions. Recombinant GST-CTD^{4A} fragment also bound less His-CTD^{WT} and even less His-CTD^{4A} (Fig. 6*d*, compare *lanes 1–3*). These results suggest a possible role of CTD in MAD1 dimerization or oligomerization (see "Discussion").

Discussion

MAD2 O–C conversion is a key signal amplification step for the mitotic checkpoint. The current model suggests that the conversion is catalyzed by an unusual catalyst: the MAD1:C-MAD2 complex localized at unattached kinetochores. How the catalysis is achieved is still unclear. Together with two very recent publications (29, 30), our results support the roles of MAD1^{CTD} and MPS1 kinase in promoting the MAD2 O–C conversion. In particular, our work agrees with the critical role

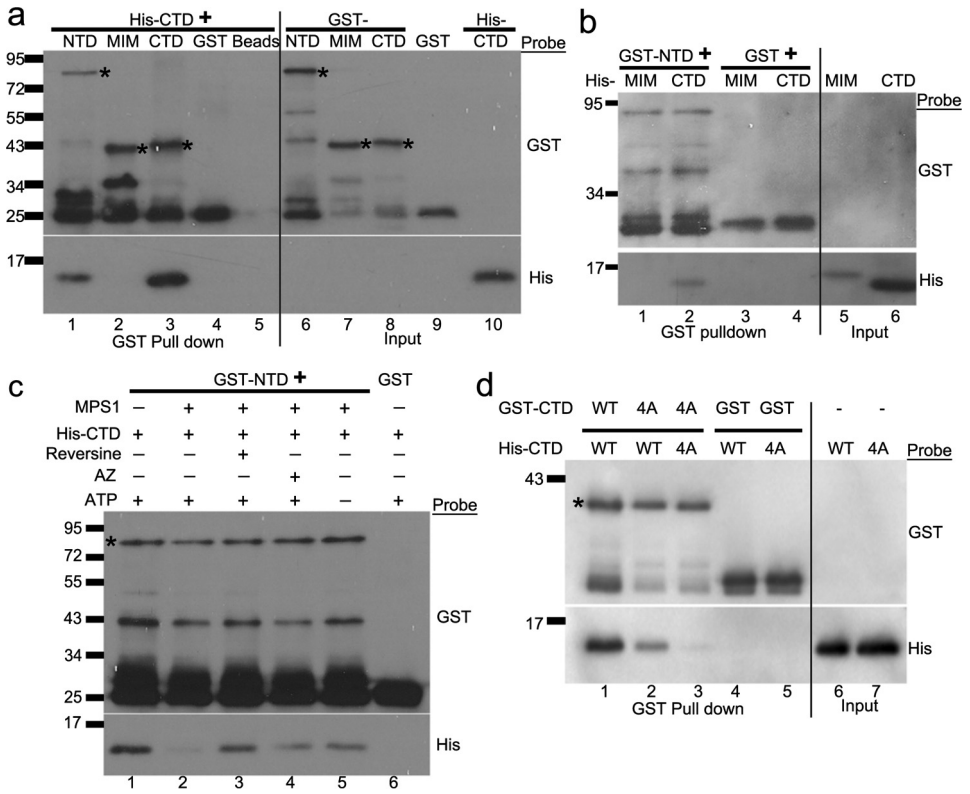

Figure 6. Interdomain interactions of MAD1 are modulated by MPS1 kinase. *a*, GST-tagged MAD1^{NTD}, MAD1^{MIM}, MAD1^{CTD}, GST (at 60 nM) or beads alone were incubated with 4 μM His-tagged MAD1^{CTD}. The GST pulldown samples were separated by SDS-PAGE and subjected to Western blotting using anti-GST and anti-His$_6$ antibodies. The *asterisks* mark the expected bands of GST-MAD1^{NTD}, MAD1^{MIM}, and MAD1^{CTD}. *b*, GST pulldown assays after GST or GST-MAD1^{NTD} was incubated with His-tagged MAD1^{MIM} and MAD1^{CTD}. *c*, recombinant GST-MAD1^{NTD} or GST alone was incubated with 9 μM His-MAD1^{CTD} in the absence or presence of MPS1 kinase, reversine (MPS1 inhibitor), AZ3146 (another MPS1 inhibitor), and ATP. GST pulldowns were then probed for anti-GST and anti-His$_6$ antibodies. The *asterisk* marks expected size of GST-NTD. *d*, GST-MAD1^{CTDWT} or GST-MAD1^{CTD4A} was incubated with His-tagged MAD1^{CTDWT} or MAD1^{CTD4A} and GST pulldowns were probed. The result has been replicated for at least three times. The *asterisk* marks expected size of GST-CTD.

of MAD1 Thr-716, which is phosphorylated by MPS1, but also suggests that Ser-610 and Tyr-634 are potentially key residues for regulating MAD2 O–C conversion (Figs. 1 and 5). Ser-610 is phosphorylated by MPS1 *in vitro* (Fig. 4), and Tyr-634 was reported to be phosphorylated *in vivo*, although we have not confirmed this yet in mitotic cells (37). We have also uncovered additional protein-protein interactions between MPS1, MAD1, and MAD2 (Figs. 2–4 and 6). Of particular interest, we found that MAD1^{NTD} and MAD1^{CTD} interact with each other and both bind to O-MAD2 and C-MAD2. These results have been integrated into an updated model for the MAD1:C-MAD2 catalyst that promotes MAD2 O–C conversion (Fig. 7). Many mechanistic details remain to be filled, so we hereby discuss the implications of our results.

The functions of MAD1^{NTD} and MAD1^{CTD} in MAD2 O–C conversion

The crystal structure of MAD1^{MIM} in complex with C-MAD2 has solidified the now classical model of the MAD1:C-MAD2 catalyst as a 2:2 heterotetramer (11) (Fig. S1). Each of the two "liganded" C-MAD2s tightly wraps around one MIM monomer through its safety belt loop (11, 18, 38). C-MAD2 then utilizes its dimerization domain to recruit O-MAD2 and converts the latter into C-MAD2, resulting in signal amplification for the mitotic checkpoint (6, 7, 12). The conversion may go through multiple intermediate states (I-MAD2) (6, 7, 10, 13, 32).

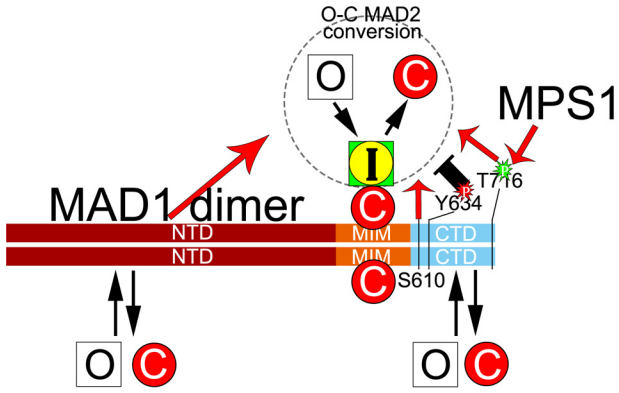

Figure 7. An updated model on the MAD1:C-MAD2 catalyst for MAD2 O–C conversion. In the classical model, a MAD1 dimer tightly binds two C-MAD2 molecules at its MIM region to become the catalyst for MAD2 O–C conversion. Our work has shown that MAD1^{NTD} and MAD1^{CTD} have additional, probably weaker, binding sites for both O-MAD2 and C-MAD2. MAD1^{NTD} and MAD1^{CTD} positively contribute to the MAD2 O–C conversion (*red arrows*), based on live cell imaging results. Several residues within the CTD domain may have important functional roles. Thr-716 phosphorylation by MPS1 and Ser-610 are required for full MAD1 activity. Tyr-634 might be a residue whose phosphorylation negatively impacts the O–C conversion. Similarly, the NTD:CTD interaction (not shown) may restrain the catalytic efficiency of MAD1, but the interaction can be disrupted by action of MPS1 kinase. It remains unclear whether the two C-MAD2 molecules bound to the MIM regions of the MAD1 dimer are equally engaged in MAD2 O–C conversion.

Although much of MAD1 has been usually simplified as rather stiff coiled coils, the known structures of MAD1^{MIM} and MAD1^{CTD} and careful analyses of MAD1^{NTD} showed that mul-

tiple MAD1 segments may adopt alternative structures or remain disordered (11, 33) (Fig. 1 and Fig. S1). It is likely that liganded C-MAD2 binding to the MIM region of MAD1 still constitutes the catalytic core and represents the MAD2 stably associated with MAD1 in cells (Fig. 1*e*), but earlier work by others has already lent strong support to possible $MAD1^{CTD}$ involvement in the mitotic checkpoint responses (12–18, 29, 30). At least part of the $MAD1^{NTD}$ contributes to MAD1 nuclear pore or kinetochore localization and interactions with other proteins including Ndc80, Plk1, Nek2A, Tpr, Cep57, and CENP-E (20–23, 33, 45–49), and the regions spanning 400–500 or 420–485 could possibly affect the mitotic checkpoint signaling (14, 29). Nevertheless, the possibility that $MAD1^{NTD}$ and $MAD1^{CTD}$ directly impact the MAD2 O–C conversion was not thoroughly studied until this work.

Our results suggest that a full-length MAD1 molecule may employ NTD and CTD to at least transiently interact with the substrates (O-MAD2), the products (C-MAD2), and even the intermediate states (I-MAD2, represented by $MAD2^{\Delta N10}$ in Fig. 3*c*) (50) of the MAD2 O–C conversion reaction. The interaction with O-MAD2 might increase local concentration of substrates, driving the conversion reaction. Similarly, enrichment of I-MAD2 by $MAD1^{NTD}$ or $MAD1^{CTD}$ could facilitate its interaction with CDC20, coupling the MAD2 O–C conversion reaction with the energy favorable assembly of the MCC (29, 30). It should be noticed that O-MAD2 conversion to C-MAD2 can certainly be accomplished in the absence of CDC20 (12, 13). Following the law of mass action, the NTD or CTD-retained C-MAD2 could also drive its interaction with BUBR1 as a step of MCC assembly (36). These possible scenarios involving $MAD1^{NTD}$ and $MAD1^{CTD}$ for C-MAD2 production and MCC assembly may underlie the compromised mitotic checkpoint responses when cells were transfected with mCherry-Mis12-$MAD1^{\Delta NTD}$ or -$MAD1^{\Delta CTD}$ (Fig. 1). Consistent with this idea, our data indicated that $MAD1^{NTD}$ and $MAD1^{CTD}$ bind to a new interface on MAD2. Such a binding mode is postulated to be advantageous, as the I-MAD2 or C-MAD2 products anchored on MAD1 could have two other protein-protein interaction interfaces, the safety belt (for CDC20) and the dimerization domain (for BUBR1), readily available to assemble the MCC. In addition, the MAD2 interactions with NTD or CTD must be weak or transient in cells, as mCherry-Mis12-$MAD1^{\Delta NTD}$ and $MAD1^{\Delta CTD}$ do not show significant reduction in co-immunoprecipitated MAD2 whereas FLAG-$MAD1^{NTD}$ only shows faint MAD2-binding (Fig. 1, *e* and *f*). Such transient interactions are likely also beneficial for stepwise relay mechanisms to facilitate MAD2 O–C conversion and MCC assembly.

In the $MAD1^{MIM}$:C-MAD2 tetramer structure (11, 32), the dimerization interfaces along the two C-MAD2 molecules to recruit O-MAD2 face toward opposite directions. It is therefore possible that endogenous full-length MAD1, when bound by C-MAD2 at MIM to form a catalyst, contains more than one catalytic center. It remains to be seen whether $MAD1^{NTD}$ and $MAD1^{CTD}$ asymmetrically affect the two presumable $MAD1^{MIM}$:C-MAD2 catalytic centers or directly contribute to the catalysis through stabilizing some transient I-MAD2 states such as those with unfolded N or C terminus (10, 13). In addition, $MAD1^{CTD}$ and $MAD1^{NTD}$ are important for MAD1 oligomerization (Figs. 1, *e* and *f*, and 6*d*). We noticed an earlier publication suggesting that Ser-214 phosphorylation by ATM affects MAD1 dimerization (51). Whether MAD1 dimerization regulates MAD2 conversion is an interesting topic for future exploration.

The impact of mitotic kinases on MAD2 O–C conversion

Whatever the catalytic mechanism the MAD1:C-MAD2 complexes employ to promote MAD2 O–C conversion, the catalysis is likely initiated or enhanced by mitotic checkpoint kinases whose activities have been shown important for the checkpoint, including MPS1, BUB1, and Aurora B (25, 26, 28, 31). These kinases not only help enrich the MAD1:C-MAD2 catalysts to unattached kinetochores, but also directly impact their catalytic efficiency. In this work we have focused on the potential effect of MPS1 on increasing the catalytic efficiency of the MAD1:C-MAD2 complex.

MPS1 is a key upstream kinase orchestrating the organization of other mitotic checkpoint proteins at unattached kinetochores. It phosphorylates KNL1 to recruit BUB1:BUB3 and BUBR1:BUB3 complexes (reviewed in Refs. 1 and 52). It also phosphorylates BUB1 to recruit MAD1:MAD2 to kinetochores (30, 31, 53). In addition, MPS1 phosphorylating MAD1 at Thr-716 may enhance MAD1 binding to CDC20 (30). Thus MPS1 activity may promote the formation of the MCC by placing all MCC components BUBR1:BUB3, CDC20, and MAD2 in spatial proximity (29, 30). CDC20 binding to BUB1 or BUBR1 might also help the MCC assembly at unattached kinetochores (54–56).

We have demonstrated that MPS1 interacts with and phosphorylates $MAD1^{NTD}$ and $MAD1^{CTD}$ (Fig. 4). Phosphoresistant mutants at *in vitro* MPS1 phosphorylation sites in $MAD1^{CTD}$, especially the T716A mutation, compromised the mitotic checkpoint responses in cells and showed reduced interaction with MAD2 *in vitro* (Fig. 5). No increase in MAD2 interactions with $MAD1^{CTD}$ was detected either using the phosphomimic T716E mutant or after direct *in vitro* phosphorylation by MPS1 (Figs. 4 and 5). We also expected to see differential bindings of O-MAD2 and C-MAD2 to $MAD1^{NTD}$ or $MAD1^{CTD}$, especially after MPS1 phosphorylation, but do not have experimental evidence to support the idea yet (Fig. 4). We cannot exclude the possibility that in cells and in the context of full-length MAD1, CTD phosphorylation shows differential binding toward either conformer of MAD2. Synergistic effect with phosphorylation by other kinases such as BUB1 and Aurora B may also be necessary to see such effects. Phosphorylation by MPS1 did reduce its own interaction with CTD and the interaction between NTD and CTD (Figs. 4 and 6).

We propose that the NTD:CTD interaction occurs in interphase cells and represents an inactive state of MAD1 even though its MIM associates with C-MAD2 in a cell cycle–independent manner (18, 24). The interaction between MPS1 and MAD1 might contribute to the MAD1 recruitment to kinetochores. Once concentrated at unattached kinetochores, MPS1 kinase becomes activated and phosphorylates BUB1 to stably anchor MAD1 (30, 31, 57). Activated MPS1 also phosphorylates $MAD1^{CTD}$, most likely at Thr-716, relieving itself and the NTD from CTD. The now exposed and phosphorylated CTD could bind to O-MAD2 and C-MAD2 and also facilitate the

MAD2 O–C conversion either directly or through increased association with CDC20 (30), as discussed in the last section.

Although deleting $MAD1^{NTD}$ compromised the mitotic checkpoint when examined using the mCherry-Mis12 fusions (Fig. 1), mutating presumable MPS1 phosphorylation sites within $MAD1^{NTD}$ had no impact on the mitotic checkpoint (Fig. 5), and others found no requirement for MAD1 N-terminal 400 or 420 residues for MAD2 O–C conversion or checkpoint responses (14, 29). This suggests that a functional critical region lies within 420–485 residues, which happens to contain a likely non–coiled-coil structure (Fig. 1). However, neither of the MAD1 fragments spanning 327–423 or 327–488 residues bind to MAD2 *in vitro* (Fig. 2), indicating the positive effect of $MAD1^{NTD}$ on the mitotic checkpoint signaling needs further clarification.

Interestingly, Faesen *et al.* (29) reported that MAD2 can be phosphorylated by MPS1 *in vitro* at Ser-195. Previously, phosphorylation at this site was proposed to render MAD2 hard to convert and thus more likely to stay in O conformation (43, 58). Whether this particular MAD2 phosphorylation by MPS1 represents a feedback regulatory mechanism can be further explored. In this regard, it might be useful to note that MPS1 interacts with C-MAD2 and O-MAD2 whereas $MAD2^{S195D}$ binds to MAD1 at NTD or CTD but not MIM, behaving indeed like an O-MAD2 (Figs. 3*a* and 4*c*).

Although recent work has proposed how BUB1 might help the MAD2 O–C conversion and MCC assembly (29–31), it will still be interesting to further define how other kinases such as Aurora B regulate the MAD1:C-MAD2 catalyst to increase C-MAD2 production. In addition, there have been reports that some tyrosine kinases help silence the mitotic checkpoint to drive anaphase onset (59–63). MAD1 Y634 seems to play important roles in the mitotic checkpoint (Fig. 1 and Fig. S4), and it was once reported to be phosphorylated *in vivo* (37). Further characterization of this site as well as the apparently essential Ser-610 and Thr-716 residues at the $MAD1^{CTD}$ will provide more mechanistic insights into the functions of MAD1 in MAD2 O–C conversion.

Experimental procedures

DNA constructs

The MAD1 and MAD2 DNA fragments and mutants used in the work are summarized in Table S1. The pMSCV-mCherry-Mis12-MAD1 constructs with wild-type or a mutant MAD1 (K541A, L543A) were gifts from Dr. Tarun Kapoor (Rockefeller University) (26, 28). Other MAD1 mutants or truncations were cloned or mutated in an intermediate pENTR2B vector (Invitrogen), cut out as a NotI-*Eco*RI fragment, and then used to replace the *MAD1* gene in the pMSCV-mCherry-Mis12 backbone also cut with NotI and *Eco*RI. Mutagenesis was conducted using QuikChange Lightning Multi Site-Directed Mutagenesis Kit (Agilent). Different fragments of MAD1 were also cloned into a pENTR/D-TOPO vector using TOPO Cloning Kit (Invitrogen) and then recombined into pDEST15 (for N-terminal GST tag) or pDEST17 (for N-terminal His_6-tag) vectors through LR reactions as instructed for the Gateway cloning system (Invitrogen). MAD2 expression constructs were prepared similarly as before (36), but with a tobacco etch virus (TEV) cleavage site inserted between the tags and second MAD2 codon during pENTR cloning steps. MPS1 was recombined into pDEST10 or pDEST20 and transformed into DH10BAC to prepare recombinant bacmids for Sf9 insect cell transfection. All constructs were confirmed by DNA sequencing.

Cell culture and transfection

HeLaM, a subline of HeLa (35), was maintained in DMEM with 10% fetal bovine serum at 37 °C in 5% CO_2. DNA transfection was carried out using TransIT-LT1 reagent (Mirus) following the manufacturer's instructions or using polyethyleneimine (PEI) as described before (64). Sf9 cells were grown at 27 °C in SFX medium (Hyclone) in the presence of antibiotics (streptomycin/penicillin). Cellfectin (Invitrogen) was used to transfect bacmids into Sf9 cells.

Live cell imaging

For determining mitotic durations, HeLa cells grown on No. 1.5 coverslip-bottomed 35-mm dishes (MatTek) were transfected with different mCherry-Mis12-MAD1 constructs. Usually 24 h after transfection, live cell imaging was started on an automated Olympus IX-81 microscope to collect phase contrast and RFP images at 15-min intervals using a 60× objective lens (NA = 1.42) while cells were maintained at 37 °C in a heating chamber. Single-plane images were acquired for up to 13 h at multiple positions using a CoolSNAP HQ2 camera with 2 × 2 binning. Student's *t* test was used to evaluate the statistical significance between the differences in mitotic durations after different treatment. Nuclear envelope breakdown marks the beginning and appearance of cleavage furrow the end of a mitosis. Some images were collected on a Leica TCS SP8 confocal microscope with a 63× objective (NA = 1.40) as *z*-stacks of 1.0 μm.

Cell lysates, immunoblotting, and immunoprecipitation

These were performed as described before (28, 64). A list of primary antibodies used in this study is summarized in Table S2.

Recombinant proteins

GST-tagged or His-tagged MAD1 fragments and His-TEV–tagged $MAD2^{L13A}$ or His-TEV–tagged $MAD2^{\Delta C10}$ were expressed in *Escherichia coli* BL21(DE3)-CodonPlus RIPL (Stratagene), normally at 16 °C. His-MPS1 or GST-MPS1 was expressed in Sf9 cells after infection with recombinant baculoviruses. All expressed proteins were purified using GSH-agarose or Probond nickel beads (Invitrogen). His-tagged TEV(S219P) protease (65) was used to cleave His-tag to make untagged MAD2. Peak fractions of eluted proteins were pooled, buffer-exchanged, and concentrated using Pierce protein concentrators with 10,000 molecular weight cutoff. The storage buffer is 50 mM Hepes pH7.5, 100 mM KCl, 1 mM DTT, 30% glycerol. Concentrations of recombinant proteins were determined by comparing the target band with BSA standards on Coomassie Blue–stained gels using ImageJ software (66).

In vitro binding assays

4 μl of 5× binding buffer (100 mM Tris-HCl, pH 8.0, 750 mM NaCl, 50 mM $MgCl_2$, 2.5% Nonidet P-40, 50% glycerol, 500 μg/ml BSA) was mixed with recombinant GST-tagged MAD1 fragments and MAD2 mutants or His-MAD1^{CTD} or His-MPS1. The proteins (including related fragments or mutants) were used at roughly endogenous intracellular concentrations unless stated otherwise in the figure legends: [MAD2] = 230 nM, [MPS1] = 100 nM, and [MAD1] = 60 nM (8, 67–69). H_2O was added to make the final volume 20 μl. The reactions were incubated at 37 °C for 1 h and then mixed with 10 μl GSH agarose beads and shaken at 800 rpm at 4 °C for 40 min (Peqlab Thriller). The beads were pelleted and washed four times with wash buffer (20 mM phosphate buffer, pH 7.4, 250 mM NaCl, 0.5% Nonidet P-40, 10% glycerol). Then 10 μl 2× SDS sample buffer was added to the beads and the samples were heated at 80 °C for 10 min before SDS-PAGE. The gel was transferred to PVDF membranes (Millipore) for immunoblotting. Most of the *in vitro* binding results have been replicated three times or more.

In vitro kinase assays

GST-tagged MPS1 kinase was purchased from Invitrogen or was purified from Sf9 cell lysates as well as His-tagged MPS1 (64). Myelin basic protein was purchased from Sigma as an artificial substrate for MPS1. *In vitro* kinase assays were set up similarly as described previously (28, 64): 4 μl of 5× kinase buffer (125 mM Tris-HCl, pH 7.5, 300 mM β-glycerophosphate, 50 mM $MgCl_2$) was mixed with recombinant kinase, substrates, 5μCi ^{32}P ATP and 50 μM cold ATP. In some reactions, MPS1 kinase inhibitors reversine (Calbiochem) or AZ3146 (Selleckchem) was used at 500 nM and 2 μM final concentrations, respectively. DMSO concentration is kept below 0.5%. H_2O was added to make the final volume 20 μl. The reactions were incubated at 30 °C for 30 min and then terminated by adding 20 μl 2× SDS sample buffer. Samples were subjected to SDS-PAGE followed by Coomassie Blue staining. After destaining, the SDS-PAGE gel was vacuum dried. Phosphorylation of the substrates was visualized by autoradiography. Samples for mass spectrometry were prepared using only 0.5 mM cold ATP in the kinase reactions and separated on SDS-PAGE. Phosphorylated residues on the excised bands were determined by mass spectrometry (MS Bioworks, Ann Arbor, MI).

For experiments shown in Fig. 4, *d* and *e*, *in vitro* kinase assays were performed by incubating GST-MPS1 and His-MAD1^{CTD} in the presence or absence of 0.5 mM cold ATP and 25 μM reversine at 30 °C for 1 h. Then untagged MAD2^{L13A} or MAD2$^{\Delta C10}$ were directly added into the reaction mixtures and incubated at 37° for another hour before immunoprecipitation with 1 μg anti-His_6 antibody.

Author contributions—W. J. and S.-T. L. conceptualization; W. J., Y. L., E. A., and S.-T. L. data curation; W. J., Y. L., E. A., and S.-T. L. formal analysis; W. J., Y. L., E. A., and S.-T. L. investigation; W. J., Y. L., E. A., and S.-T. L. methodology; W. J., Y. L., E. A., and S.-T. L. writing-review and editing; S.-T. L. supervision; S.-T. L. funding acquisition; S.-T. L. writing-original draft; S.-T. L. project administration.

Acknowledgments—We thank Drs. Tarun Kapoor and Maria Maldonado for the mCherry-Mis12-MAD1-WT and -AA constructs and Dr. Tim Yen for multiple antibodies. We also thank Dr. William Taylor, Dr. Qian Chen and the members of the Liu lab for stimulating discussions.

References

1. Musacchio, A. (2015) The molecular biology of spindle assembly checkpoint signaling dynamics. *Curr. Biol.* **25,** R1002–R1018 CrossRef Medline
2. London, N., and Biggins, S. (2014) Signalling dynamics in the spindle checkpoint response. *Nat. Rev. Mol. Cell Biol.* **15,** 736–747 CrossRef Medline
3. Lara-Gonzalez, P., Westhorpe, F. G., and Taylor, S. S. (2012) The spindle assembly checkpoint. *Curr. Biol.* **22,** R966–R980 CrossRef Medline
4. Liu, S. T., and Zhang, H. (2016) The mitotic checkpoint complex (MCC): looking back and forth after 15 years. *AIMS Molecular Science* **3,** 597–634 CrossRef Medline
5. Rieder, C. L., Cole, R. W., Khodjakov, A., and Sluder, G. (1995) The checkpoint delaying anaphase in response to chromosome monoorientation is mediated by an inhibitory signal produced by unattached kinetochores. *J. Cell Biol.* **130,** 941–948 CrossRef Medline
6. Luo, X., and Yu, H. (2008) Protein metamorphosis: The two-state behavior of Mad2. *Structure* **16,** 1616–1625 CrossRef Medline
7. Mapelli, M., and Musacchio, A. (2007) MAD contortions: Conformational dimerization boosts spindle checkpoint signaling. *Curr. Opin. Struct. Biol.* **17,** 716–725 CrossRef Medline
8. Luo, X., Tang, Z., Xia, G., Wassmann, K., Matsumoto, T., Rizo, J., and Yu, H. (2004) The Mad2 spindle checkpoint protein has two distinct natively folded states. *Nat. Struct. Mol. Biol.* **11,** 338–345 CrossRef Medline
9. Fava, L. L., Kaulich, M., Nigg, E. A., and Santamaria, A. (2011) Probing the *in vivo* function of Mad1:C-Mad2 in the spindle assembly checkpoint. *EMBO J.* **30,** 3322–3336 CrossRef Medline
10. Hara, M., Özkan , E., Sun, H., Yu, H., and Luo, X. (2015) Structure of an intermediate conformer of the spindle checkpoint protein Mad2. *Proc. Natl. Acad. Sci. U.S.A.* **112,** 11252–11257 CrossRef Medline
11. Sironi, L., Mapelli, M., Knapp, S., De Antoni, A., Jeang, K. T., and Musacchio, A. (2002) Crystal structure of the tetrameric Mad1-Mad2 core complex: Implications of a 'safety belt' binding mechanism for the spindle checkpoint. *EMBO J.* **21,** 2496–2506 CrossRef Medline
12. De Antoni, A., Pearson, C. G., Cimini, D., Canman, J. C., Sala, V., Nezi, L., Mapelli, M., Sironi, L., Faretta, M., Salmon, E. D., and Musacchio, A. (2005) The Mad1/Mad2 complex as a template for Mad2 activation in the spindle assembly checkpoint. *Curr. Biol.* **15,** 214–225 CrossRef Medline
13. Yang, M., Li, B., Liu, C. J., Tomchick, D. R., Machius, M., Rizo, J., Yu, H., and Luo, X. (2008) Insights into mad2 regulation in the spindle checkpoint revealed by the crystal structure of the symmetric mad2 dimer. *PLoS Biol.* **6,** e50 CrossRef Medline
14. Kruse, T., Larsen, M. S., Sedgwick, G. G., Sigurdsson, J. O., Streicher, W., Olsen, J. V., and Nilsson, J. (2014) A direct role of Mad1 in the spindle assembly checkpoint beyond Mad2 kinetochore recruitment. *EMBO Rep.* **15,** 282–290 CrossRef Medline
15. Heinrich, S., Sewart, K., Windecker, H., Langegger, M., Schmidt, N., Hustedt, N., and Hauf, S. (2014) Mad1 contribution to spindle assembly checkpoint signalling goes beyond presenting Mad2 at kinetochores. *EMBO Rep.* **15,** 291–298 CrossRef Medline
16. Ballister, E. R., Riegman, M., and Lampson, M. A. (2014) Recruitment of Mad1 to metaphase kinetochores is sufficient to reactivate the mitotic checkpoint. *J. Cell Biol.* **204,** 901–908 CrossRef Medline
17. Kuijt, T. E., Omerzu, M., Saurin, A. T., and Kops, G. J. (2014) Conditional targeting of MAD1 to kinetochores is sufficient to reactivate the spindle assembly checkpoint in metaphase. *Chromosoma* **123,** 471–480 CrossRef Medline
18. Chen, R. H., Brady, D. M., Smith, D., Murray, A. W., and Hardwick, K. G. (1999) The spindle checkpoint of budding yeast depends on a tight com-

plex between the Mad1 and Mad2 proteins. *Mol. Biol. Cell* **10,** 2607–2618 CrossRef Medline
19. Kulukian, A., Han, J. S., and Cleveland, D. W. (2009) Unattached kinetochores catalyze production of an anaphase inhibitor that requires a Mad2 template to prime Cdc20 for BubR1 binding. *Dev. Cell* **16,** 105–117 CrossRef Medline
20. Chen, R. H., Shevchenko, A., Mann, M., and Murray, A. W. (1998) Spindle checkpoint protein Xmad1 recruits Xmad2 to unattached kinetochores. *J. Cell Biol.* **143,** 283–295 CrossRef Medline
21. Rodriguez-Bravo, V., Maciejowski, J., Corona, J., Buch, H. K., Collin, P., Kanemaki, M. T., Shah, J. V., and Jallepalli, P. V. (2014) Nuclear pores protect genome integrity by assembling a premitotic and mad1-dependent anaphase inhibitor. *Cell* **156,** 1017–1031 CrossRef Medline
22. Akera, T., Goto, Y., Sato, M., Yamamoto, M., and Watanabe, Y. (2015) Mad1 promotes chromosome congression by anchoring a kinesin motor to the kinetochore. *Nat. Cell Biol.* **17,** 1124–1133 CrossRef Medline
23. Martin-Lluesma, S., Stucke, V. M., and Nigg, E. A. (2002) Role of hec1 in spindle checkpoint signaling and kinetochore recruitment of mad1/mad2. *Science* **297,** 2267–2270 CrossRef Medline
24. Campbell, M. S., Chan, G. K., and Yen, T. J. (2001) Mitotic checkpoint proteins HsMAD1 and HsMAD2 are associated with nuclear pore complexes in interphase. *J. Cell Science* **114,** 953–963 Medline
25. Hewitt, L., Tighe, A., Santaguida, S., White, A. M., Jones, C. D., Musacchio, A., Green, S., and Taylor, S. S. (2010) Sustained Mps1 activity is required in mitosis to recruit O-Mad2 to the Mad1-C-Mad2 core complex. *J. Cell Biol.* **190,** 25–34 CrossRef Medline
26. Maldonado, M., and Kapoor, T. M. (2011) Constitutive Mad1 targeting to kinetochores uncouples checkpoint signalling from chromosome biorientation. *Nat. Cell Biol.* **13,** 475–482 CrossRef Medline
27. Tighe, A., Staples, O., and Taylor, S. (2008) Mps1 kinase activity restrains anaphase during an unperturbed mitosis and targets Mad2 to kinetochores. *J. Cell Biol.* **181,** 893–901 CrossRef Medline
28. Tipton, A. R., Ji, W., Sturt-Gillespie, B., Bekier, M. E., 2nd, Wang, K., Taylor, W. R., and Liu, S. T. (2013) Monopolar Spindle 1 (MPS1) Kinase Promotes Production of Closed MAD2 (C-MAD2) Conformer and Assembly of the Mitotic Checkpoint Complex. *J. Biol. Chem.* **288,** 35149–35158 CrossRef Medline
29. Faesen, A. C., Thanasoula, M., Maffini, S., Breit, C., Müller, F., van Gerwen, S., Bange, T., and Musacchio, A. (2017) Basis of catalytic assembly of the mitotic checkpoint complex. *Nature* **542,** 498–502 CrossRef Medline
30. Ji, Z., Gao, H., Jia, L., Li, B., and Yu, H. (2017) A sequential multi-target Mps1 phosphorylation cascade promotes spindle checkpoint signaling. *Elife* **6,** e22513 Medline
31. Zhang, G., Kruse, T., López-Méndez, B., Sylvestersen, K. B., Garvanska, D. H., Schopper, S., Nielsen, M. L., and Nilsson, J. (2017) Bub1 positions Mad1 close to KNL1 MELT repeats to promote checkpoint signalling. *Nat. Commun.* **8,** 15822 CrossRef Medline
32. Mapelli, M., Massimiliano, L., Santaguida, S., and Musacchio, A. (2007) The Mad2 conformational dimer: structure and implications for the spindle assembly checkpoint. *Cell* **131,** 730–743 CrossRef Medline
33. Kim, S., Sun, H., Tomchick, D. R., Yu, H., and Luo, X. (2012) Structure of human Mad1 C-terminal domain reveals its involvement in kinetochore targeting. *Proc. Natl. Acad. Sci. U.S.A.* **109,** 6549–6554 CrossRef Medline
34. Hardwick, K. G., and Murray, A. W. (1995) Mad1p, a phosphoprotein component of the spindle assembly checkpoint in budding yeast. *J. Cell Biol.* **131,** 709–720 CrossRef Medline
35. Tipton, A. R., Tipton, M., Yen, T., and Liu, S. T. (2011) Closed MAD2 (C-MAD2) is selectively incorporated into the mitotic checkpoint complex (MCC). *Cell cycle* **10,** 3740–3750 CrossRef Medline
36. Tipton, A. R., Wang, K., Link, L., Bellizzi, J. J., Huang, H., Yen, T., and Liu, S. T. (2011) BUBR1 and closed MAD2 (C-MAD2) interact directly to assemble a functional Mitotic checkpoint complex. *J. Biol. Chem.* **286,** 21173–21179 CrossRef Medline
37. Rikova, K., Guo, A., Zeng, Q., Possemato, A., Yu, J., Haack, H., Nardone, J., Lee, K., Reeves, C., Li, Y., Hu, Y., Tan, Z., Stokes, M., Sullivan, L., Mitchell, J., *et al.* (2007) Global survey of phosphotyrosine signaling identifies oncogenic kinases in lung cancer. *Cell* **131,** 1190–1203 CrossRef Medline
38. Luo, X., Tang, Z., Rizo, J., and Yu, H. (2002) The Mad2 spindle checkpoint protein undergoes similar major conformational changes upon binding to either Mad1 or Cdc20. *Mol. Cell* **9,** 59–71 CrossRef Medline
39. Sironi, L., Melixetian, M., Faretta, M., Prosperini, E., Helin, K., and Musacchio, A. (2001) Mad2 binding to Mad1 and Cdc20, rather than oligomerization, is required for the spindle checkpoint. *EMBO J.* **20,** 6371–6382 CrossRef Medline
40. Luo, X., Fang, G., Coldiron, M., Lin, Y., Yu, H., Kirschner, M. W., and Wagner, G. (2000) Structure of the Mad2 spindle assembly checkpoint protein and its interaction with Cdc20. *Nat. Struct. Biol.* **7,** 224–229 CrossRef Medline
41. Yang, M., Li, B., Tomchick, D. R., Machius, M., Rizo, J., Yu, H., and Luo, X. (2007) p31comet blocks Mad2 activation through structural mimicry. *Cell* **131,** 744–755 CrossRef Medline
42. Chao, W. C., Kulkarni, K., Zhang, Z., Kong, E. H., and Barford, D. (2012) Structure of the mitotic checkpoint complex. *Nature* **484,** 208–213 CrossRef Medline
43. Kim, S., Sun, H., Ball, H. L., Wassmann, K., Luo, X., and Yu, H. (2010) Phosphorylation of the spindle checkpoint protein Mad2 regulates its conformational transition. *Proc. Natl. Acad. Sci. U.S.A.* **107,** 19772–19777 CrossRef Medline
44. Santaguida, S., Tighe, A., D'Alise, A. M., Taylor, S. S., and Musacchio, A. (2010) Dissecting the role of MPS1 in chromosome biorientation and the spindle checkpoint through the small molecule inhibitor reversine. *J. Cell Biol.* **190,** 73–87 CrossRef Medline
45. Lince-Faria, M., Maffini, S., Orr, B., Ding, Y., Florindo, C., Sunkel, C. E., Tavares, A., Johansen, J., Johansen, K. M., and Maiato, H. (2009) Spatiotemporal control of mitosis by the conserved spindle matrix protein Megator. *J. Cell Biol.* **184,** 647–657 CrossRef Medline
46. Lee, S. H., Sterling, H., Burlingame, A., and McCormick, F. (2008) Tpr directly binds to Mad1 and Mad2 and is important for the Mad1-Mad2-mediated mitotic spindle checkpoint. *Genes Dev.* **22,** 2926–2931 CrossRef Medline
47. Chi, Y. H., Haller, K., Ward, M. D., Semmes, O. J., Li, Y., and Jeang, K. T. (2008) Requirements for protein phosphorylation and the kinase activity of polo-like kinase 1 (Plk1) for the kinetochore function of mitotic arrest deficiency protein 1 (Mad1). *J. Biol. Chem.* **283,** 35834–35844 CrossRef Medline
48. Lou, Y., Yao, J., Zereshki, A., Dou, Z., Ahmed, K., Wang, H., Hu, J., Wang, Y., and Yao, X. (2004) NEK2A interacts with MAD1 and possibly functions as a novel integrator of the spindle checkpoint signaling. *J. Biol. Chem.* **279,** 20049–20057 CrossRef Medline
49. Zhou, H., Wang, T., Zheng, T., Teng, J., and Chen, J. (2016) Cep57 is a Mis12-interacting kinetochore protein involved in kinetochore targeting of Mad1-Mad2. *Nat. Commun.* **7,** 10151 CrossRef Medline
50. Paul, A. S., and Pollard, T. D. (2008) The role of the FH1 domain and profilin in formin-mediated actin-filament elongation and nucleation. *Curr. Biol.* **18,** 9–19 CrossRef Medline
51. Yang, C., Hao, J., Kong, D., Cui, X., Zhang, W., Wang, H., Guo, X., Ma, S., Liu, X., Pu, P., and Xu, B. (2014) ATM-mediated Mad1 serine 214 phosphorylation regulates Mad1 dimerization and the spindle assembly checkpoint. *Carcinogenesis* **35,** 2007–2013 CrossRef Medline
52. Lischetti, T., and Nilsson, J. (2015) Regulation of mitotic progression by the spindle assembly checkpoint. *Mol. Cell Oncol.* **2,** e970484 CrossRef Medline
53. London, N., and Biggins, S. (2014) Mad1 kinetochore recruitment by Mps1-mediated phosphorylation of Bub1 signals the spindle checkpoint. *Genes Dev.* **28,** 140–152 CrossRef Medline
54. Di Fiore, B., Davey, N. E., Hagting, A., Izawa, D., Mansfeld, J., Gibson, T. J., and Pines, J. (2015) The ABBA motif binds APC/C activators and is shared by APC/C substrates and regulators. *Dev. Cell* **32,** 358–372 CrossRef Medline
55. Diaz-Martinez, L. A., Tian, W., Li, B., Warrington, R., Jia, L., Brautigam, C. A., Luo, X., and Yu, H. (2015) The Cdc20-binding Phe box of the spindle checkpoint protein BubR1 maintains the mitotic checkpoint complex during mitosis. *J. Biol. Chem.* **290,** 2431–2443 CrossRef Medline
56. Lischetti, T., Zhang, G., Sedgwick, G. G., Bolanos-Garcia, V. M., and Nilsson, J. (2014) The internal Cdc20 binding site in BubR1 facilitates both

spindle assembly checkpoint signalling and silencing. *Nat. Commun.* **5,** 5563 CrossRef Medline

57. Kang, J., Chen, Y., Zhao, Y., and Yu, H. (2007) Autophosphorylation-dependent activation of human Mps1 is required for the spindle checkpoint. *Proc. Natl. Acad. Sci. U.S.A.* **104,** 20232–20237 CrossRef Medline
58. Wassmann, K., Liberal, V., and Benezra, R. (2003) Mad2 phosphorylation regulates its association with Mad1 and the APC/C. *EMBO J.* **22,** 797–806 CrossRef Medline
59. St-Denis, N., Gupta, G. D., Lin, Z. Y., Gonzalez-Badillo, B., Veri, A. O., Knight, J. D. R., Rajendran, D., Couzens, A. L., Currie, K. W., Tkach, J. M., Cheung, S. W. T., Pelletier, L., and Gingras, A. C. (2016) Phenotypic and interaction profiling of the human phosphatases identifies diverse mitotic regulators. *Cell Rep.* **17,** 2488–2501 CrossRef Medline
60. Moasser, M. M., Srethapakdi, M., Sachar, K. S., Kraker, A. J., and Rosen, N. (1999) Inhibition of Src kinases by a selective tyrosine kinase inhibitor causes mitotic arrest. *Cancer Res.* **59,** 6145–6152 Medline
61. Wolanin, K., Magalska, A., Kusio-Kobialka, M., Podszywalow-Bartnicka, P., Vejda, S., McKenna, S. L., Mosieniak, G., Sikora, E., and Piwocka, K. (2010) Expression of oncogenic kinase Bcr-Abl impairs mitotic checkpoint and promotes aberrant divisions and resistance to microtubule-targeting agents. *Mol. Cancer Ther.* **9,** 1328–1338 CrossRef Medline
62. Caron, D., Byrne, D. P., Thebault, P., Soulet, D., Landry, C. R., Eyers, P. A., and Elowe, S. (2016) Mitotic phosphotyrosine network analysis reveals that tyrosine phosphorylation regulates Polo-like kinase 1 (PLK1). *Sci. Signal.* **9,** rs14 CrossRef Medline
63. Elowe, S. (2017) Tyr(less) kinase signaling during mitosis. *Cell Cycle* **16,** 746–748 CrossRef Medline
64. Ji, W., Arnst, C., Tipton, A. R., Bekier, M. E., 2nd, Taylor, W. R., Yen, T. J., and Liu, S. T. (2016) OTSSP167 abrogates mitotic checkpoint through inhibiting multiple mitotic kinases. *PLoS One* **11,** e0153518 CrossRef Medline
65. Kapust, R. B., Tözsér, J., Fox, J. D., Anderson, D. E., Cherry, S., Copeland, T. D., and Waugh, D. S. (2001) Tobacco etch virus protease: Mechanism of autolysis and rational design of stable mutants with wild-type catalytic proficiency. *Protein Eng.* **14,** 993–1000 CrossRef Medline
66. Schneider, C. A., Rasband, W. S., and Eliceiri, K. W. (2012) NIH Image to ImageJ: 25 years of image analysis. *Nat. Meth.* **9,** 671–675 CrossRef Medline
67. Fang, G. (2002) Checkpoint protein BubR1 acts synergistically with Mad2 to inhibit anaphase-promoting complex. *Mol. Biol. Cell* **13,** 755–766 CrossRef Medline
68. Tang, Z., Bharadwaj, R., Li, B., and Yu, H. (2001) Mad2-Independent inhibition of APCCdc20 by the mitotic checkpoint protein BubR1. *Dev. Cell* **1,** 227–237 CrossRef Medline
69. Howell, B. J., Moree, B., Farrar, E. M., Stewart, S., Fang, G., and Salmon, E. D. (2004) Spindle checkpoint protein dynamics at kinetochores in living cells. *Curr. Biol.* **14,** 953–964 CrossRef Medline